Organic Dielectric Films for Flexible Transistors as Gas Sensors

Dennis C. García[1], José E. E. Izquierdo[1], Vinicius A. M. Nogueira[1], José D. S. Oliveira[1], Marco R. Cavallari[1,2], Alain A. Quivy[3] and Fernando J. Fonseca [1]

[1] Escola Politécnica da Universidade de São Paulo (EPUSP) - São Paulo, Brazil
[2] Universidade Federal da Integração Latino-Americana (UNILA), Engenharia de Energia - Foz do Iguaçu, Brazil,
[3] Institute of Physics, University of Sao Paulo, Rua do Matao 1371, 05508-090 Sao Paulo, SP, Brazil,
e-mail: fjfonseca@usp.br

***Abstract*— Cross-linked polymer films with poly(melamine-co-formaldehyde) methylated (PMF) were investigated in order to integrate flexible organic transistor-based sensors. A dielectric film that withstands lithography of the electrodes and semiconductor deposition is necessary in order to form bottom-gate/bottom-contact thin-film transistors. This device structure makes it possible to fabricate integrated circuits, while exposing the semiconductor to gaseous analytes. For the first time, films from poly(methyl methacrylate) (PMMA) blended with PMF were shown chemically resistant to wet processing. However, thin-films from poly (4-vinylphenol) (PVP) blends with PMF featured lower RMS roughness (0.37 nm) and higher dielectric constant ($k \sim 4.7 – 5.9$). The presence of enhanced cross-linking at higher PMF concentrations was confirmed for both polymers from chemical resistance essays, structural characterization, and capacitors with fully-photopatterned electrodes.**

***Index Terms*—flexible electronics, organic electronics, PVP, PMMA, PMF.**

I. Introduction

Organic electronic devices benefit from optical transparency, mechanical flexibility, large area and potential low-cost processing [1]. A bottom-gate/bottom-contact organic thin-film transistor structure as shown in Fig. 1 is desirable, since it allows the semiconductor to be exposed to a target gaseous analyte. Although not flexible, organic thin-film transistors (OTFTs) can be processed over highly-doped silicon or glass. The former is usually provided with a thermally-grown SiO_2. This dielectric features a smooth surface (RMS roughness of ca. 0.2 nm), low leakage current (~10 nA/cm^2 at 0.2 MV/cm), and a breakdown electric field higher than 10 MV/cm [2,3]. In addition, it can withstand photolithography of source and drain electrodes, as well as semiconductor deposition. This oxide, however, is brittle, opaque, expensive and processed over 1,000 °C [2]. Furthermore, the substrate acts as a common gate electrode for all transistors and a self-assembled monolayer (SAM) is still required to decrease charge carrier trapping and, consequently, enhance the effective mobility in the semiconducting channel [4,5]. A glass substrate, on the other hand, demands for an alternative dielectric material to replace SiO_2. However, some of the mentioned challenges persist, such as withstanding electrodes and semiconductor processing, while providing an interface with reduced charge trapping [6].

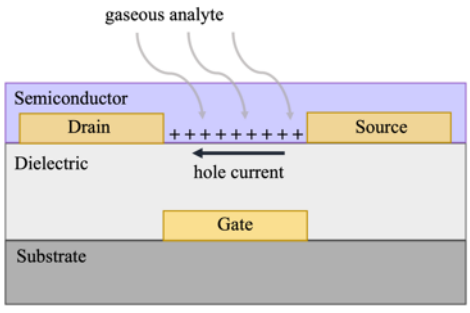

Fig.1 Schematic of the interaction between gaseous analyte molecules and charges in the channel of a bottom gate bottom contact organic transistor.

Among the most studied dielectric molecules to integrate OTFTs, poly (4-vinylphenol) (PVP) and poly(methyl methacrylate) (PMMA) are among the most promising [6,7]. Processing on top of an organic gate dielectric film in bottom gate structures requires, however, cross-linking of polymer chains [8]. OTFTs from PVP blended to poly(melamine-co-formaldehyde) methylated (PMF) have been demonstrated in the past decades [1,6,8]. Nevertheless, it is not clear if films from higher concentrations of the cross-linker agent provide better field-effect devices with photopatterned electrodes. In addition, cross-linked films of PMMA:PMF for organic electronics still remains unexplored. In this context, this work is an in-depth investigation to correlate surface and morphological characterizations with electrical performance in capacitors from cross-linked polymers. It opens up the possibility to integrate these dielectric films to OTFTs as gas sensors.

II. Materials and Methods

A. Fabrication details

Substrates were BK7 glass square slides (Opto Eletrônica S/A, São Carlos, Brazil), except for Fourier-transform infrared (FTIR) spectroscopy. In this case, silicon wafers (p-type, B-doped, <100>, 10 – 20 Ω.cm, 3-inch diameter, 14 – 16 mil thick, prime grade) were used. Cleaning was performed in sequential baths in acetone, deionized (DI) water, and isopropyl alcohol, followed by blow dry in N_2. PVP (Mw = 25 kg/mol, Aldrich) and PMMA (MicroChem 950 A6, 6 wt.% in anisole) were cross-linked with PMF (Mn ~432, 84 wt. % in 1-butanol, Aldrich) at 1:1 and 1:5 ratio (r). Polymers were dissolved in propylene glycol methyl ether acetate (PGMEA) (Mn = 132,16 g/mol, 99,5 %, Aldrich) at 6.4 – 35 wt.% concentrations (c) and deposited by spin coating (P–6000, SCS Inc.) at 1,000 – 4,000 rpm for 60 s. Organic films were dried at 100 ºC for 10 min and cross-linked at 175 ºC for 120 min on a hot plate.

Metal films for capacitors were 5 nm-thick nickel:chromium (Ni:Cr) adhesion layer followed by 95 nm-thick gold layer by DC sputtering. Electrodes were patterned by photolithography followed by etching. For that, a 1.2 µm-thick layer of positive AZ1518 photoresist (Clariant, NJ, USA)

Digital Object Identifier 10.29292/jics.v15i2.170

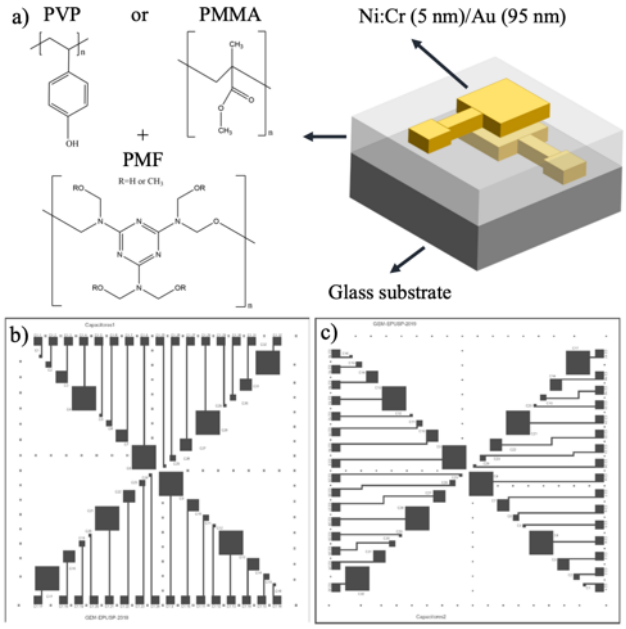

Fig.2 Parallel-plate organic capacitors: (a) schematics of device structure and materials; and photomasks for (b) bottom and (c) top electrodes.

was spun at 3000 rpm for 30 s. It was pre-baked at 80 °C for 20 min to be later exposed to a 350 W UV mercury lamp for 6 s in a Karl Süss KG mask aligner. Development was performed by immersion in AZ351, diluted at 1:5 in DI water, for 30 s. Finally, post-baking was performed at 100 °C for 30 min in another oven. Gold was etched at 1 µm/min rate for 5 s, in a bath of potassium iodide (KI) with iodine (I_2) in DI water at 4 g : 1 g : 40 mL and 30 °C. Ni:Cr was etched at 60 nm/min for 10 s in cerium (IV) ammonium nitrate ($Ce(NH_4)_2(NO_3)_6$) in perchloric acid ($HClO_4$) and DI water at 10 : 5 : 85 volumetric ratio and at ca. 27 °C. Photoresist was removed in a sequence of baths exactly as in the initial cleaning process.

Device structure and the chemical structure of organic molecules are presented in Fig. 2(a). Photomasks for patterning both bottom and top capacitor electrodes are shown in Fig. 2(b) and (c), respectively. Capacitor area (A) is defined by the overlapping of squares with sides of 25, 50, 100, and 200 µm. The sequence of steps to fabricate organic capacitors is given in Fig. 3.

B. Chemical resistance

In order to check thin-film resistance to opening vias in integrated circuits, polymer films were oxygen plasma etched at 100 W, 100 mTorr and 50 sccm (Plasmalab TTL, Plasma Technology, UK). In addition, 500 µL of organic solvents, such as toluene (TOL), chlorobenzene (CB), dichlorobenzene (DCB), and chloroform (CF), were dispensed with a micropipette on top of polymer films and spun at 2,000 rpm for 60 s. Solvent and spinning parameters emulate usual values for organic semiconducting deposition [9-11]. Thickness (d) was monitored with an Alpha step 100 profilometer (Veeco, NY, USA) after gently scratching the films.

C. Surface and structural characterization

Thin-film RMS roughness (Rq) was investigated in 5 x 5 µm^2 surface area by atomic force microscopy (AFM, Bruker NanoScope® IIIA). Chemical bonds were addressed by Raman (532 nm laser wavelength, 45 mW power, Confocal Raman Microscope Alpha 300 R, WITec, Germany) and FTIR (5 kHz frequency, QS-300 FTS-40 (BIO-RAD, USA) spectroscopies. All measurements were taken at room temperature and 1 atm pressure.

D. Electrical measurements

Breakdown voltage (E_{bd}) and leakage current ($J_{leakage}$) were extracted from current versus voltage (IxV) data taken from a B1500A semiconductor parameter analyzer (Keysight, USA). Capacitance (C) data was also acquired with a B1500A (1 kHz and ±1 V). The dielectric constant (k) was calculated from the parallel-plate capacitor model:

$$C = \varepsilon_0 kA/d \tag{2}$$

where ε_0 is the vacuum permittivity.

III. Results And Discussion

A. Investigation of spin-coated thin-film thickness

PVP:PMF films from 1:1/16 wt.% solutions featured a thickness of 644 – 1,335 nm depending on the spinning frequency in Fig. 4(a). After increasing the ratio to 1:5, while keeping the concentration constant, film thickness decreased to 177 – 333 nm. A pure PVP film from a less concentrated solution (6.4 wt.%) was prepared in order to understand the effect of PMF addition to thin-film thickness. The obtained values were comparable to PVP:PMF at 1:5. Therefore, PMF addition tends to bring close together PVP molecules and,

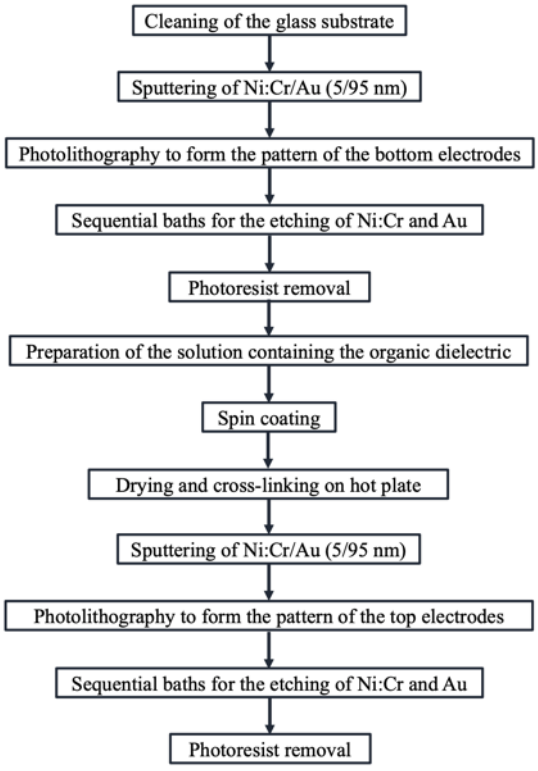

Fig.3 Sequence of processing steps for capacitor fabrication.

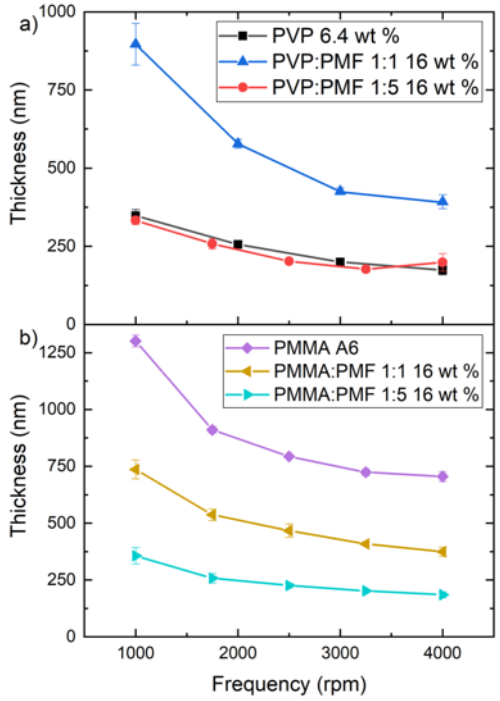

Fig.4 Thin-film thickness versus spin coating frequency of (a) PVP and (b) PMMA solutions

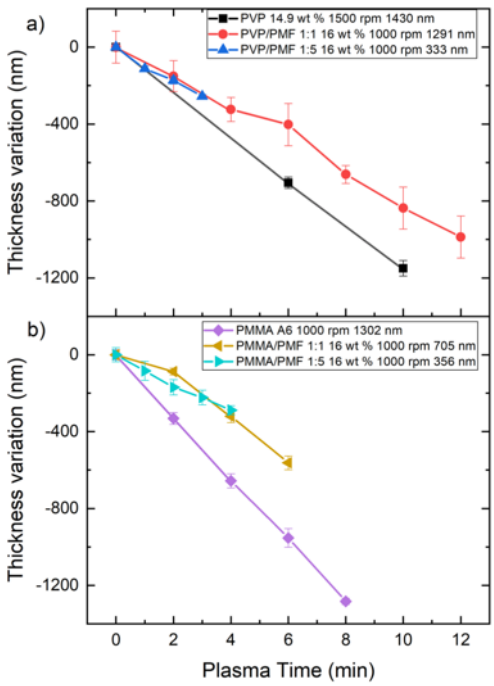

Fig.5 Thickness variation as a function of O_2 plasma etching time for (a) PVP and (b) PMMA films

consequently, form a more compact and dense film [9].

A similar behavior is observed for PMMA:PMF films in Fig. 4(b). Even though the concentration is the same, increasing PMF mass ratio with respect to PMMA brings down thickness by a factor of two. It decreases from 374 – 735 nm to 185 – 357 nm. In this case, however, less-concentrated pure PMMA solutions seem to have higher viscosity, since films are thicker for all processing frequencies and 1,302 nm-thick films at 1,000 rpm show defects even with bare eyes.

B. Chemical resistance in oxygen plasma and organic solvent environments

Thin-film thickness variation as a function of O_2-plasma etching time is given in Fig. 5. Note that thinner films have less data points, since it gets fully etched after a shorter time compared to thicker ones. Among films without the cross-linking agent, PVP has a lower etching rate (115 ± 16 nm/min) compared to PMMA (160 ± 3 nm/min). By adding PMF to PVP at 1:1 mass ratio, there is a decrease of approx. 28 % of the etching rate. Further increasing PMF ratio does not alter the etching rate (83 ± 15 nm/min). At this ratio, PMMA:PMF showed the highest resistance to O_2-plasma etching (71 ± 10 nm/min). Even though cross-linked films are harder to etch and, consequently, to open vias in integrated circuits, these results corroborate the presence of cross-linking already at 1:1 ratio.

Thin-film resistance to organic solvents is shown in Fig. 6. Heating of the solvents prior to spin coating derives from the need to deposit organic semiconductors from low-volatile solvents. Despite an enhancement in film crystallinity from a slow drying, heating is mandatory due to a poor solubility in these solvents [9,11,12]. PVP:PMF films at 1:1 ratio tend to thin down after spin coating of room-temperature DCB, CB, and TOL. An increase in thickness after exposure to CF points to thin-film bloating. By heating the solvents prior to spinning, an even more aggressive dissolution was expected. In this case, however, films tend to bloat in DCB, TOL, and CF. The absence of a drying step after solvent spin

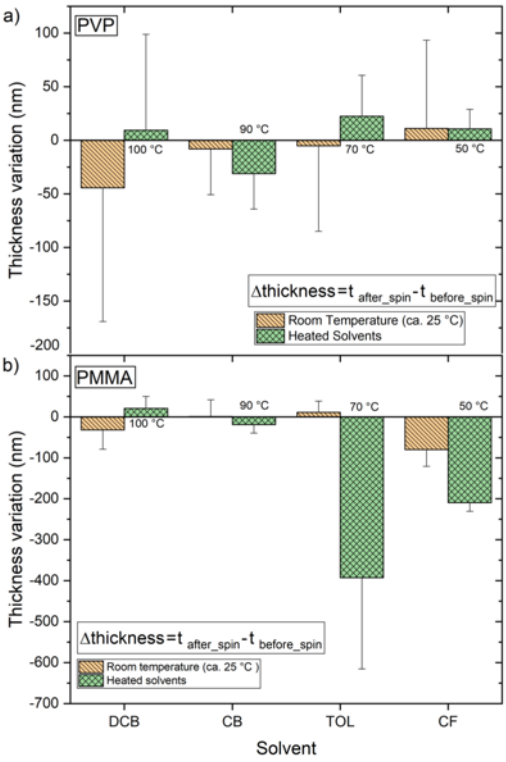

Fig.6 Change in thickness of (a) PVP and (b) PMMA thin-films at 1:1 ratio with PMF after spin coating of solvents.

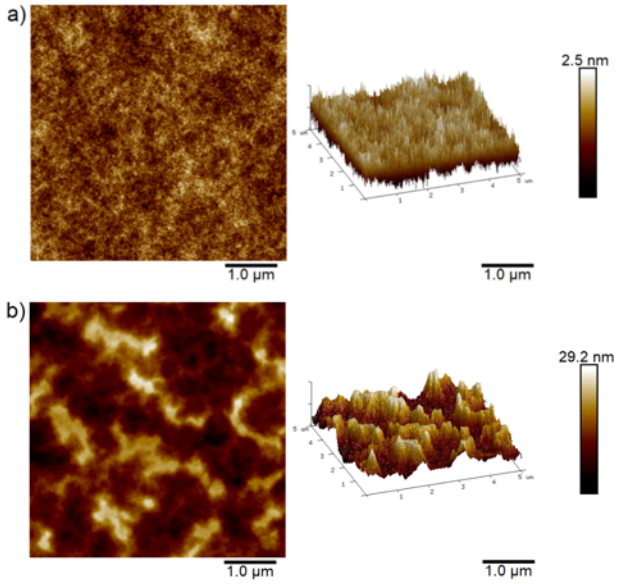

Fig.7 AFM micrographs of cross-linked (a) PVP and (b) PMMA films

coating could explain why the thickness increase in some cases. However, by taking into account that the change in thickness is smaller than the error bar, one could conclude that PVP:PMF films could withstand spin coating of the semiconductor solution to form bottom-gate OTFTs.

Similar to cross-linked PVP films, PMMA:PMF at 1:1 ratio resisted to room-temperature DCB, CB, and TOL. After heating TOL, however, the decrease in thickness was higher than the error bar. Even worse, CF dissolved PMMA:PMF even at room temperature. These results are, nevertheless, promising for semiconductors deposited from DCB and CB solutions [9]. It is worth mentioning that these thickness variations are expected to be even lower at 1:5 ratio, due to enhanced cross-linking. The authors believe the higher chemical resistance of films at 1:5 ratio to O_2 plasma etching should also be observed against exposure to organic solvents.

C. Surface and morphological characterization

The addition of PMF to PVP films tend to form more compact and rougher films [8]. PVP:PMF at 1:1 ratio in Fig. 7(a) showed a 0.37 nm *Rq*, which is comparable to previous results [6]. PMMA:PMF at the same ratio in Fig. 7(b) featured a 6.8 nm *Rq*. A rougher film could be originating from a lower spinning frequency of 1,000 rpm. Higher rotating speeds are advised to OTFTs, since semiconducting film thickness can be even lower than 20 nm [10,11].

According to FTIR results in Fig. 8(a), PVP:PMF films at 1:1 ratio showed a strong presence of a band at 1,481 cm^{-1} attributed to CH_2 and CH_3 groups [13], as well as bands at 2,960 and 3,410 cm^{-1} assigned to the stretching vibration of C-H and O-H groups, respectively [14,15]. These bands tend to decrease and, in some cases, disappear with an increase in the PMF ratio. In the opposite trend, there was an increase in bands at 810 cm^{-1} related to the triazine ring-sextant out-of-plane bending [13], 1,372 cm^{-1} attributed to C-N groups [16,17], 1,558 cm^{-1} from C–N bonds directly attached to the triazine ring [13], and 1,072 cm^{-1} due to C-O-C out-of-phase stretching modes [13,18]. The observed behavior at these bands is a sign of enhanced cross-linking in the film. The absorption peak at 2,360 cm^{-1} is believed to be due to the presence of environmental carbon dioxide (CO_2) inside the spectrometer during data acquisition [19,20].

Similar observations can be made for PMMA films in Fig. 8(b). There is an increase in bands attributed to C-N and C-O-C groups. Even for these films, there was CO_2 during the measurements. In particular, PMMA-based films featured bands at 1,728 cm^{-1} related to the stretching vibration band of C=O, and 2,960 cm^{-1} from O-CH_3 (stretching vibration) and C-CH_3 (asymmetric vibration) bonds [21]. Higher cross-linking at higher mass ratios agrees well with results from plasma etching.

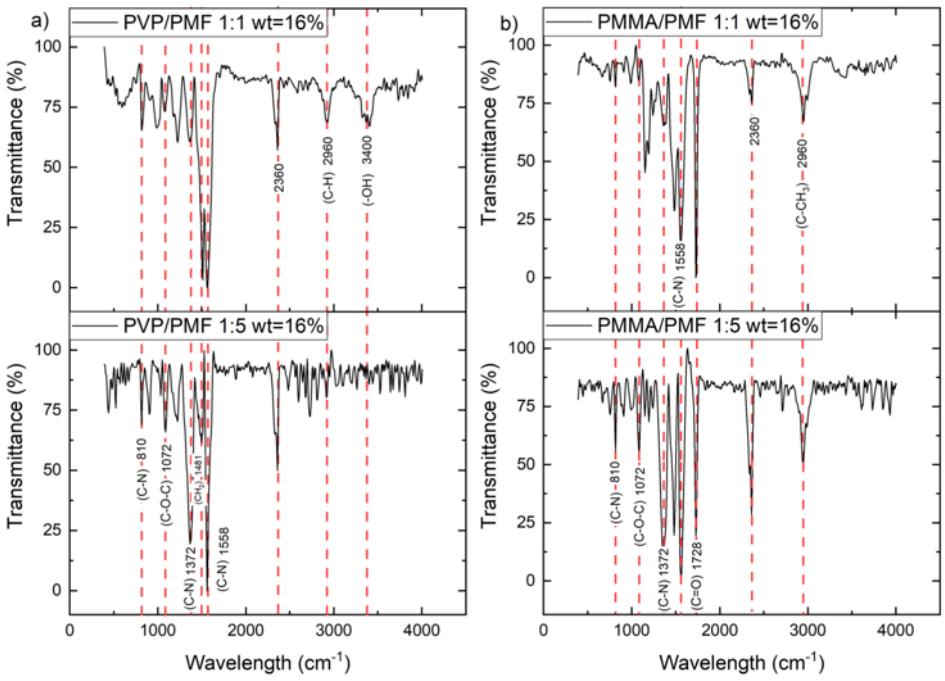

Fig.8 FTIR spectra of (a) PVP and (b) PMMA films

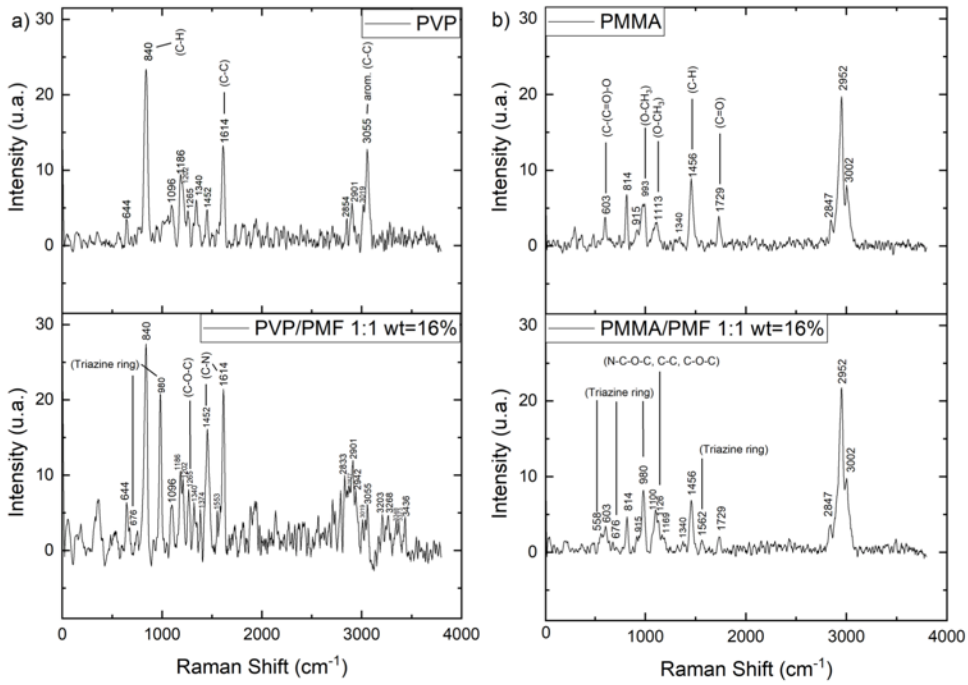

Fig.9 Raman spectra of (a) PVP and (b) PMMA films

Raman spectra of PVP-based films are shown in Fig. 9(a). Typical bands from the PVP molecules are at 840 cm^{-1} from out-of-plane C-H deformation, and 1,614 cm^{-1} related to C-C bonds in the phenyl group [22]. By increasing the PMF concentration with respect to PVP, the intensity of the band at 1,614 cm^{-1} increases due to C-N groups from the triazine ring in PMF [13]. In addition, there is an increase of the bands at 1,265 and 1,452 cm^{-1} related to C-O-C [22,23] and C-N [13,23] groups, respectively. As for FTIR, these are a sign of enhanced cross-linking at higher PMF ratios. New peaks arise at 676 from in-plane bending of C-N bonds exogenous to the triazine ring [13,23,24], 980 cm^{-1} due to the triazine ring breathing vibration [24], and 1,553 cm^{-1} from contraction of the C–N bond directly attached to the ring [13,23]. They relate to the triazine ring from the PMF molecule. By considering the fact PVP-based films are hygroscopic [25], peaks between 3,200 and 3,400 cm^{-1} can relate to the presence of water molecules during data acquisition [26-28].

Raman spectra from PMMA-based films as shown in Fig. 9(b) featured peaks at: (*i*) 603 cm^{-1} related to C-(C=O)-O deformation [21,22]; (*ii*) 993 and 1,113 cm^{-1} from O-CH_3 [21]; (*iii*) 1,456 cm^{-1} due to C-H bonds [21]; and (*iv*) 1,729 cm^{-1} from hydrogen-bonded C=O. PMF incorporation to the film gave rise to peaks at 558, 676, 980 [13,24], and 1,562 cm^{-1} [13] attributed to the triazine ring. By increasing PMF concentration with respect to PMMA, peaks at 993 and 1,113 cm^{-1} were replaced with peaks at 1,100, 1,126, and 1169 cm^{-1} originating from N-C-O-C, C-C and C-O-C groups, respectively [13,23].

In conclusion, these results point to a more pronounced cross-linking at a 1:5 ratio for both molecules. An illustration of the chemical structure of cross-linked polymers is given in Fig. 10. It is worth noting that, while the chemical reaction with PMF is known for PVP [29], this work is pioneer for PMMA.

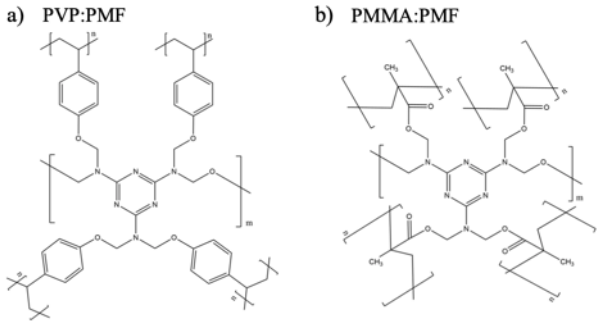

Fig.10 Illustration of the structure of cross-linked polymers with PMF.

D. Electrical characterization of capacitors

Table I summarizes the electrical performance of capacitors from cross-linked organic dielectric films. These values were obtained from capacitance density (C_d) and leakage current ($J_{leakage}$) plots as shown in Figs. 11 and 12, respectively. Differently from the thickness values given in Fig. 4, organic dielectric films to fabricate capacitors were formed on a surface containing bottom gold electrodes. A concentration of 35 wt.% in PGMEA was chosen for films from 1:5. Typical dielectric thin-film thickness values for organic transistors as gas sensors are usually higher than 200 nm [12,30-32].

PVP:PMF-based devices featured a less-dispersive data with $C_d \sim 2 - 14$ nF/cm^2 and $k \sim 4.7 - 5.9$. These values are typical for high-*k* cross-linked organic dielectrics [33,34]. Devices from a 1:5 ratio featured a higher dielectric constant, but also higher leakage currents, which are a sign of enhanced cross-linking [1,34]. In the absence of cross-linking, photolithography of electrodes tends to damage the dielectric film. On the other hand, a higher cross-linking density generates a more defective and, consequently, porous film. Although a higher surface area is desirable for gas sensing applications, if the leakage current gets too high, an additional

Table I. Summary of the electrical performance of capacitors from polymer dielectrics.

Dielectric	*r* / *c* (wt.%)	*d* (nm)	C_d (nF/cm²)	*k*	$J_{leakage}$ (nA/cm²) @ 0.2 MV/cm	E_{bd} (MV/cm)
PVP:PMF	1:1 / 16	691 ± 12	6.1 ± 0.2	4.7 ± 0.3	1×10^{-1} – 3×10^{3}	0.11 – 0.42
		342 ± 8	14 ± 1	5.2 ± 0.5	5×10^{-1} – 1×10^{3}	0.26 – 0.75
	1:5 / 35	2303 ± 50	2.3 ± 0.2	5.9 ± 0.7	1×10^{4} – 2×10^{5}	> 0.18
		1005 ± 34	4.9 ± 0.2	5.6 ± 0.4	$(4.7 \pm 1.6)\times10^{4}$	> 0.44
PMMA:PMF	1:1 / 16	691 ± 23	14 – 111	11 – 86	–	–
		352 ± 2	7.1 ± 0.6	2.8 ± 0.2	–	–
	1:5 / 35	2351 ± 90	2 – 12	4 – 32	–	–
		524 ± 39	7.2 ± 1.0	4.3 ± 0.6	–	–

insulating layer may be necessary for proper transistor operation [35]. Currently, the main strategy to enhance sensitivity is to add a porogen material to the semiconductor solution [30-32]. That so-called porogen material either decomposes after a thermal treatment [31] or is washed off the semiconducting film [30,32]. It is worth noting that a decrease in the concentration of hydroxyl groups in cross-linked PVP as shown in Fig. 10 is also beneficial to diminish charge trapping at the dielectric/semiconductor interface in OTFTs [6]. Comparable breakdown electric fields were obtained for all devices.

Data from thicker PMMA:PMF films deposited at 1,000 rpm featured a large dispersion among capacitors from the same sample. Films obtained at low rotating frequency were visually non-uniform in thickness (data not shown). In addition, PMMA:PMF films from a lower ratio seem not to completely withstand damage from the photolithographic process. As a matter of fact, the lowest *k* (~ 2.8) was observed for PMMA:PMF capacitors at 1:1 ratio. Previous reports on cross-linked PMMA with different cross-linking agents featured a *k* of 3.7 – 3.9 [7,36,37], which agrees well with PMMA:PMF at 1:5 spun at 4,000 rpm. Note, however, that the closest results are from a completely different device. Li et al. functionalized PMMA with propargyl and azido groups by free radical copolymerization [36]. Cross-linking was induced by the thermal azide–alkyne cycloaddition reaction at 100 °C. In addition, metal evaporation through a shadow mask was used to pattern the electrodes.

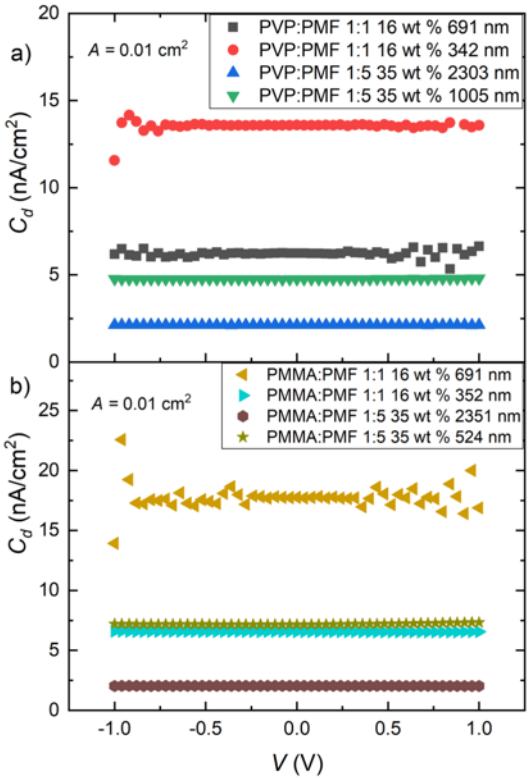

Fig.11 Capacitance density (C_d) versus DC biasing voltage (V) for capacitors from (a) PVP:PMF and (b) PMMA:PMF films.

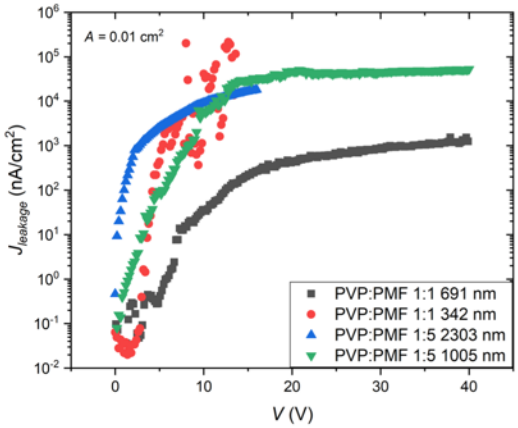

Fig.12 Leakage current ($J_{leakage}$) versus DC biasing voltage (V) for capacitors from PVP:PMF films.

In summary, the devices herein were demonstrated compatible with photopatterned bottom electrodes and semiconductor deposition for low-voltage OTFTs as gas sensors. Since the highest processing temperature is 175ºC, these dielectric films are also compatible with most mechanically flexible substrates [38].

Conclusions

Cross-linking of both studied polymers after PMF addition was verified from chemical resistance essays and structural characterization. Photopatterned high-*k* capacitors from both blends were demonstrated. The best electrical performances were observed for capacitors deposited from solutions at 1:5 ratio and spun at higher spinning frequencies. Despite being the first demonstration of device feasibility from PMMA:PMF films, PVP-based films were considered more adequate to integrate bottom-gate/bottom-contact organic transistors. They featured a reduced surface roughness, a higher resistance to organic solvents, and a higher dielectric constant. Replacing oxidized silicon wafers with chemically-resistant organic dielectric films will make it possible to fabricate flexible, transparent, integrated circuit-based and potential low-cost sensors with fully-photopatterned electrodes.

Acknowledgements

This work was supported by the Brazilian agencies

Coordenação de Aperfeiçoamento de Pessoal de Nível Superior (CAPES 88882.333362/2019-01), Conselho Nacional de Desenvolvimento Científico e Tecnológico (CNPq 168249/2018-9), and Fundação de Amparo à Pesquisa do Estado de São Paulo (FAPESP 2013/19420-0 and 13/50440-7). Special thanks are given to the cleanroom staff at LME, EPUSP, Brazil.

REFERENCES

[1] H.-J. Yun et al, "Additive effect of poly (4-vinylphenol) gate dielectric in organic thin film transistor at low temperature process," *Journal of nanoscience and nanotechnology,* vol.13, no.5, 2013, pp. 3313-3316.

[2] A.H. Carim, and A. Bhattacharyya, "Si/SiO_2 interface roughness: structural observations and electrical consequences," *Applied Physics Letters*, vol. 46, no. 9, 1985, pp. 872-874.

[3] G. Zhang, P. Zhang, H. Chen, and T. Guo, "Modification of polymer gate dielectrics for organic thin-film transistor from inkjet printing," *Applied Physics A*, vol. 124, no. 7, 2018, pp. 481.

[4] M. Lafkioti et al., "Graphene on a hydrophobic substrate: doping reduction and hysteresis suppression under ambient conditions," *Nano Letters*, vol. 10, no. 4, 2010, pp. 1149-1153.

[5] X. Zhang et al., "Ultrasensitive Field-Effect Biosensors Enabled by the Unique Electronic Properties of Graphene," *Small*, vol. 16, no. 15, 2020, pp. 1902820.

[6] H. Kim et al., "An effective method to minimize the leakage current in organic thin-film transistors by using blends of various molecular weights," *Organic Electronics,* vol.13, no.7, 2012, pp. 1255-1260.

[7] Y. Yun, C. Pearson, D.H. Cadd, R.L. Thompson, and M.C. Petty, "A cross-linked poly (methyl methacrylate) gate dielectric by ion-beam irradiation for organic thin-film transistors," *Organic Electronics*, vol.10, no. 8, 2009, pp. 1596-1600.

[8] D.-H. Kang et al., "Poly-4-vinylphenol (PVP) and poly (melamine-co-formaldehyde)(PMF)-based atomic switching device and its application to logic gate circuits with low operating voltage," *ACS Applied Materials & Interfaces,* vol. 9, no. 32, 2017, pp. 27073-27082.

[9] M.R. Cavallari et al., "Cross-linked polyvinyl phenol as dielectric for flexible bottom gate bottom contact transistors," in 4th Symposium on Microelectronics Technology and Devices (SBMicro), 2019, IEEE, pp. 1-3.

[10] V.R. Zanchin et al., "Low Voltage Organic Devices with High-k TiOxNy and PMMA Dielectrics for Future Application on Flexible Electronics," *ECS Transactions,* vol.39, no.1, 2011, pp. 455.

[11] M.R. Cavallari et al., "On the performance degradation of poly (3-hexylthiophene) field-effect transistors," *IEEE Transactions on Device and Materials Reliability,* vol.15, no.3, 2015, pp.342-351.

[12] M.R. Cavallari et al., "Enhanced Sensitivity of Gas Sensor Based on Poly(3-hexylthiophene) Thin-Film Transistors for Disease Diagnosis and Environment Monitoring," *Sensors*, vol. 15, 2015, pp. 9592-9609.

[13] P.J. Larkin, M.P. Makowski, N.B. Colthup, and L.A. Flood, "Vibrational analysis of some important group frequencies of melamine derivatives containing methoxymethyl, and carbamate substituents: mechanical coupling of substituent vibrations with triazine ring modes," *Vibrational Spectroscopy*, vol. 17, no. 1, 1998, pp. 53-72.

[14] S.C. Lim et al., "Hysteresis of pentacene thin-film transistors and inverters with cross-linked poly (4-vinylphenol) gate dielectrics," *Applied Physics Letters*, vol. 90, no. 17, 2007, pp. 173512.

[15] Y.S. Choe et al., "Crosslinked polymer-mixture gate insulator for high-performance organic thin-film transistors," *Organic Electronics*, vol. 36, 2016, pp. 171-176.

[16] I. Karamancheva et al., "FTIR spectroscopy and FTIR microscopy of vacuum-evaporated polyimide thin films," *Vibrational Spectroscopy*, vol. 19, no. 2, 1999, pp. 369-374.

[17] D. Garcia, and T.T. Serafini, "FTIR studies of PMR-15 polyimides," *Journal of Polymer Science Part B: Polymer Physics*, vol. 25, no. 11, 1987, pp. 2275-2282.

[18] R.E. Smith, F.N. Larsen, and C.L. Long, "Epoxy resin cure. II. FTIR analysis," *Journal of Applied Polymer Science*, vol. 29, no. 12, 1984, pp. 3713-3726.

[19] H.A. Ma et al., "High-pressure pyrolysis study of $C_3N_6H_6$: a route to preparing bulk C_3N_4," *Journal of Physics: Condensed Matter*, vol. 14, no. 44, 2002, pp. 11269

[20] Y.C. Zhao, D.L. Yu, H.W. Zhou, Y.J. Tian, and O. Yanagisawa, "Turbostratic carbon nitride prepared by pyrolysis of melamine," *Journal of Materials Science*, vol. 40, no. 9-10, 2005, pp. 2645-2647.

[21] G. Steiner, and C. Zimmerer, "Poly (methyl methacrylate)(PMMA)," in *Polymer Solids and Polymer Melts–Definitions and Physical Properties I*, Springer, 2013, pp. 571-582.

[22] Y. Ren et al., "Two-dimensional Fourier-transform-Raman and near-infrared correlation spectroscopy studies of poly (methyl methacrylate) blends: 2. Partially miscible blends of poly (methyl methacrylate) and poly (4-vinylphenol)," *Vibrational Spectroscopy*, vol. 23, no. 2, 2000, pp. 207-218.

[23] D. Lin-Vien, N.B. Colthup, W.G. Fateley, and J.G. Grasselli, "Triazine [1,3,5]," in *The handbook of infrared and Raman characteristic frequencies of organic molecules*, Elsevier, San Diego, 1991, pp. 300-302.

[24] M.L. Scheepers et al., "Determination of free melamine content in melamine-formaldehyde resins by Raman spectroscopy," *Vibrational Spectroscopy*, vol. 9, no. 2, 1995, pp. 139-146.

[25] H.G. Sandberg, T.G. Bäcklund, R. Österbacka, and H. Stubb, "High-Performance All-Polymer Transistor Utilizing a Hygroscopic Insulator," *Advanced Materials*, vol. 16, no. 13, 2004, pp.1112-1115.

[26] P. Talik, P. Moskal, L.M. Proniewicz, and A. Wesełucha-Birczyńska, "The Raman Spectroscopy Approach to the Study of Water–Polymer Interactions in Hydrated Hydroxypropyl Cellulose (HPC)," *Journal of Molecular Structure*, vol. 1210, 2020, pp. 128062.

[27] M. Ahmed, A.K. Singh, and J.A. Mondal, "Hydrogen-bonding and vibrational coupling of water in a hydrophobic hydration shell as observed by Raman-MCR and isotopic dilution spectroscopy," *Physical Chemistry Chemical Physics*, vol. 18, no. 4, 2016, pp. 2767-2775.

[28] M. Kačuráková, P.S. Belton, R.H. Wilson, J. Hirsch, and A. Ebringerová, "Hydration properties of xylan-type structures: an FTIR study of xylooligosaccharides," *Journal of the Science of Food and Agriculture*, vol. 77, no. 1, 1998, pp. 38-44.

[29] C. Tozlu, and A. Mutlu, "Poly (melamine-co-formaldehyde) methylated effect on the interface states of metal/polymer/p-Si Schottky barrier diode," *Synthetic Metals*, vol. 211, 2016, pp. 99-106.

[30] S. Wu et al., "Organic Field-Effect Transistors with Macroporous Semiconductor Films as High-Performance Humidity Sensors," *ACS Applied Materials & Interfaces*, vol. 9, 2017, pp. 14974-14982.

[31] K. Besar, J. Dailey, and H.E. Katz, "Ethylene Detection Based on Organic Field-Effect Transistors With Porogen and Palladium Particle Receptor Enhancements," *ACS Applied Materials & Interfaces*, vol. 9, 2017, pp. 1173–1177.

[32] M.S. Park, A.A. Meresa, C.M. Kwon, F.S. Kim, "Selective Wet-Etching of Polymer/Fullerene Blend Films for Surface- and Nanoscale Morphology-Controlled Organic Transistors and Sensitivity-Enhanced Gas Sensors," *Polymers*, vol. 11, 2019, pp. 1682.

[33] F.Y. Yang, M.Y Hsu, G.W. Hwang, and K.J. Chang, "High-performance poly (3-hexylthiophene) top-gate transistors incorporating TiO_2 nanocomposite dielectrics," *Organic Electronics*, vol. 11, no. 1, 2010, pp. 81-88.

[34] S. Singh, and Y.N. Mohapatra, "Dielectric optimization for inkjet-printed TIPS-pentacene organic thin-film transistors," *IEEE 2nd International Conference on Emerging Electronics (ICEE),* December, 2014, pp. 1-4.

[35] F. Zhang, G. Qu, E. Mohammadi, J. Mei, Y. Diao, "Solution-Processed Nanoporous Organic Semiconductor Thin Films: Toward Health and Environmental Monitoring of Volatile Markers," *Advanced Functional Materials*, vol. 27, 2017, pp. 1701117.

[36] S. Li, L. Feng, J. Zhao, X. Guo, and Q. Zhang, "Low temperature cross-linked, high performance polymer gate dielectrics for solution-processed organic field-effect transistors," *Polymer Chemistry*, vol. 6, no. 32, 2015, pp. 5884-5890.

[37] S. Jung et al., "A TIPS-TPDO-tetraCN-based n-type organic field-effect transistor with a cross-linked PMMA polymer gate dielectric," *ACS Applied Materials & Interfaces*, vol. 8, no. 23, 2016, pp. 14701-14708.

[38] W.A. MacDonald et al., "Latest advances in substrates for flexible electronics," *Journal of the Society for Information Display*, vol. 15, no. 12, 2007, pp.1075-1083.